Title: Natural selection imposed by mechanical properties of a biomaterial results in novel cellular phenotypes

Authors: Purboja Purkayastha[1], Kavya Pendyala[1], Ayush S. Saxena[2], Hesamedin Hakimjavadi[3], Srikar Chamala[3], Charles F. Baer[2,3], and Tanmay P. Lele[1*]

Affiliations:

[1] Department of Chemical Engineering, University of Florida, Gainesville FL 32611, USA

[2] Department of Biology, University of Florida, Gainesville FL 32611, USA

[3] University of Florida Genetics Institute, Gainesville FL 32611, USA

*Correspondence to: Tanmay P. Lele, Department of Chemical Engineering, University of Florida, Gainesville FL 32611, USA. Email: tlele@che.ufl.edu; Charles F. Baer, Department of Biology, University of Florida, Gainesville FL 32611, USA. Email: cbaer@ufl.edu.

Abstract: The physical properties of biomaterials – such as stiffness or nanostructure- are commonly tailored to direct cell functions in diverse applications. While biochemically induced laboratory cellular evolution is well established, no studies have examined whether population of cells can evolve in response to selection pressure imposed by the physical properties of biomaterials. Here we found that genetically variable populations of fibroblasts increased in fitness upon sustained culture on novel soft biomaterial substrates, whereas clonal populations did not. Whole exome-sequencing combined with simulations of experimental evolution revealed that cells evolved by natural selection and not random drift. Novel cell phenotypes were observed on the soft substrate upon evolution, and different replicate lines evolved the same phenotypes through distinct patterns of gene expression. These results suggest that laboratory cellular evolution on biomaterials is a powerful untapped approach that can be used to generate cell populations with novel genetic and phenotypic properties.

One Sentence Summary: Genetically variable populations of cells evolve upon sustained culture on a soft substrate to produce novel phenotypes.

Main Text:

Strategies to engineer lifelike tissues must utilize biomaterial substrates of appropriate physical properties such as stiffness, not only for achieving optimal tissue stiffness and integration but also for establishing the desired phenotypes and functions of cells that adhere to the scaffold (*1-4*). While engineering cell fitness has been proposed to be a potentially useful strategy in tissue engineering (*5*), in contrast to the many studies that have demonstrated cellular evolution in response to biochemical signals (e.g. antibiotics), there are no studies that have examined whether physical properties of the environment can exert selection pressure to cause cellular evolution. This is particularly germane to biomaterials whose physical properties – such as stiffness or nanostructure- are commonly tailored to direct cell functions in diverse applications.

In the terminology of evolutionary biology, the alternative phenotypes that arise due to substrate stiffness among cells with identical underlying genotypes is called "phenotypic plasticity". The proximate cause of phenotypic plasticity is epigenetic change (e.g., DNA methylation, changes to small RNAs), here induced by substrates of defined stiffness which can be heritable in the short term (*6-8*). The ultimate cause of the plastic response itself is likely natural selection, a hypothesis which predicts that the specific phenotypes manifested in environments of different stiffnesses should have higher fitness than the alternative phenotype. It should therefore be possible at least in principle to generate cell populations with novel phenotypic properties by allowing cell populations containing sufficient genetic variation to evolve on biomaterials of different stiffnesses. This strategy may not necessarily result in cells with novel properties if evolution by natural selection has already resulted in cells that are optimally adapted to both the

stiff and the soft substrate. In that case, sustained culture of a genetically variable cellular population on each of the substrates would simply result in purifying selection at the level of the genome and stabilizing selection at the level of the phenotype. This scenario is depicted by the pink line in **Fig. 1**, "perfect trait", and there is no possibility of generating novel cellular phenotypes in this scenario.

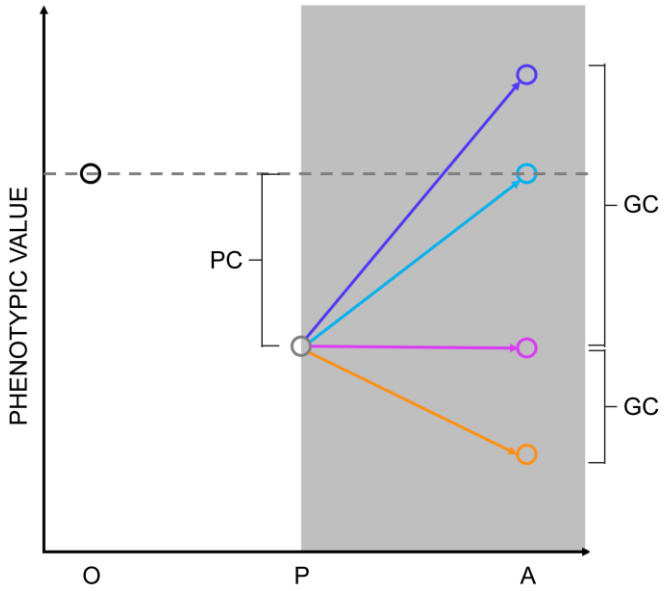

Fig. 1. Relationship between plasticity and evolutionary outcomes. X-axis labels: O represents the phenotypic value of the ancestor on the stiff substrate; P represents the plastic phenotypic value of the ancestor on the soft substrate and A represents the phenotypic value after evolution on the soft substrate. PC designates plastic change", GC designates "genetic change" (see text). The arrows represent potential outcomes; orange arrow, “evolutionary head start”; pink arrow, “perfect trait”; light blue arrow, “revert to normal”, and dark blue arrow, “maladaptive plasticity”. Phenotypic values different from the plastic phenotype are novel outcomes that could result from cellular evolution on biomaterials.

Evolutionary biologists commonly assume that phenotypic plasticity takes the phenotype in the direction favored by natural selection (*9*), with the implication that sustained selection in one condition will take the phenotype further in the direction of the plastic response (orange line in **Fig.1**; "evolutionary head start"), i.e., plasticity is immediately adaptive. But the opposite could also be true: short-term plastic responses in a genetically variable population could be opposed by long-term adaptive evolution (blue lines in **Fig. 1**, "return to normal" or even "maladaptive plasticity"(*10*)). Either of these outcomes would generate new types of evolved cells and would be of interest in biomaterial applications.

Accordingly, we asked which of the evolutionary possibilities illustrated in **Fig. 1** best characterizes cellular evolution on biomaterials of defined stiffnesses. We used an experimental evolution system, wherein murine fibroblasts adapted *in vitro* to growth on a rigid substrate (tissue culture plastic) were evolved on a soft substrate.

Results

Cellular evolution on soft substrates

For the evolution experiments, we chose NIH 3T3 fibroblasts, which have been maintained in culture on a stiff substrate (i.e., tissue culture plastic dishes) for decades and are a well-established model system for studying sensitivity to substrate stiffness (*11-14*). Considering their long evolutionary history, these cells are expected to be at or near population genetic equilibrium. Ten replicate lines were initiated by plating ~10^4 cells on soft polyacrylamide gels (E = 1 kPa) and six replicate lines on stiff (E = 308 kPa) polyacrylamide gels (**Fig. 2A**; the two specific values of stiffnesses were chosen because these cells exhibit considerable phenotypic plasticity on these two substrates (*15*)). These lines were allowed to grow for approximately three days and then 10^4 cells

were passaged onto fresh substrates of the same (corresponding) stiffness (**Fig. 2A;** cell doubling times were roughly 1-2 days). This procedure was carried out for 3 months, i.e., for approximately 90 cell generations. As a measure of fitness, we determined the cellular growth rate at one-month intervals over the course of the experiment (see supplemental methods).

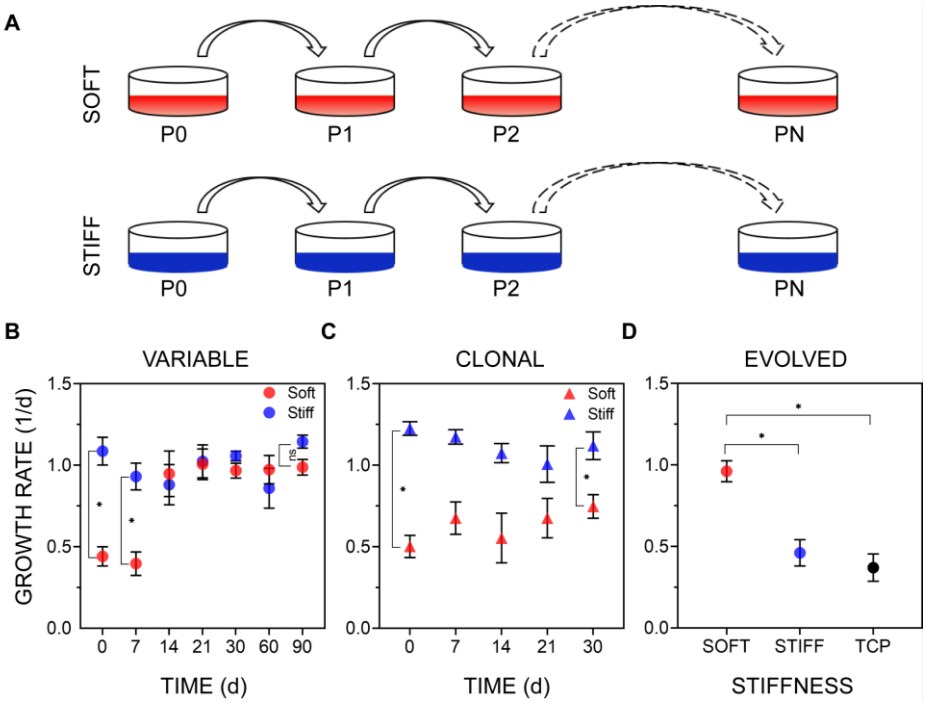

Fig. 2. Evidence of evolution on soft substrates in murine fibroblasts. (A) Overview of the evolution experiment. Cells were cultured on the soft (red, E = 1 kPa) or stiff substrate (blue, E = 308 kPa) for up to 90 d. (B) The mean growth rate of selected lines on the soft and stiff substrates, measured at different times during sustained 90-d culture. Error bars, SEM; data were collected from lines which were derived from the genetically variable ancestral population and were then cultured on the soft substrate (at least eight independent lines), or the stiff substrate (at least six independent lines). Statistically significant differences were determined by Mann-Whitney U test, *$P < 0.05$; ns: $P > 0.05$. (C) The mean growth rate of lines derived from clonal cells determined

at different times during sustained culture. Error bars, SEM; data were collected from eight or more different clonal populations. Statistically significant differences were determined by Mann-Whitney U test, *$P < 0.05$. (D) The mean growth rate of soft-selected lines on stiff substrates. Four lines were derived from the genetically variable ancestral population and then cultured for 90 d on the soft substrate. These selected lines were then cultured on soft or stiff substrates (TCP, tissue culture plastic) and their growth rate was measured on these substrates over 3 days of culture. Error bars, SEM. Statistical significance was determined by Kruskal-Wallis test followed Dunn's multiple comparison test; *$P < 0.05$.

Consistent with previous studies (*16*), the growth rate of cells on the soft substrate was initially nearly two-fold lower than that on the stiff substrate (**Fig. 2B**). After 30 days of culture on the soft substrate, the growth rate had approximately doubled and become indistinguishable from the growth rate on the stiff substrate for the remainder of the experiment (**Fig. 2B**). However, we did not know precisely when this change occurred within the first 30 days, nor whether it was gradual or abrupt. To establish the early dynamics, we repeated these experiments for 9 replicate lines on the soft substrate and 10 replicate lines on the stiff substrate, and measured the growth rate at 7-day intervals. The growth rate of the lines on the soft substrate increased rapidly in approximately 2-3 weeks of culture, becoming statistically indistinguishable from the growth rate of lines on the stiff substrate.

To establish the generality of this observation, we conducted a similar experiment with a different cell type, murine C2C12 myoblasts, which also have been maintained on a stiff substrate (tissue culture plastic) for decades and thus are also expected to be at or near an evolutionary equilibrium. The myoblast mean growth rate on the soft substrate (n=6 lines) was initially lower than that of the same cells on the stiff substrate (n=6 lines). Over the course of 2 months, the

growth rate of the cells on soft substrate had again evolved to be statistically indistinguishable from the growth rate on the stiff substrate (**Fig. S1**). These observations indicate that the fitness of genetically variable starting cell lines can and does respond over the course of a few weeks to selection imposed by a novel substrate.

Adaptation requires genetic variation for selection to act upon. Accordingly, we tested whether or not clonal cell lines also increased in fitness over time. We repeated these experiments with clonal fibroblast lines initiated from individual cells (see supplemental methods), which are expected to be genetically homogeneous. Growth rate in these populations did not change over the course of 4 weeks (**Fig. 2C**). Thus, a genetically variable source population is required for an increase in growth rate on the soft substrate, consistent with our interpretation that the change in growth rate is the result of evolution.

Unless selection is extraordinarily strong (e.g., as in the case of antibiotic exposure leading to drug resistance in bacterial culture), one would not expect that detectable evolutionary changes would occur on the timescale of a few cell divisions. The observed rapid evolution of growth rate on the soft (novel) substrate in the variable but not the clonal lines, combined with the two-fold difference in ancestral growth rate between the two substrates, has two implications regarding the evolved cells: (1) these cellular genotypes are present and rare in the ancestral population; and also (2) these cells grow slowly on the stiff substrate. Consistent with the second prediction, we found that soft-evolved cells grew slower on the stiff substrate (308-kPa gels as well as tissue culture plastic) than on the soft substrate (**Fig. 2D**).

With respect to the second prediction (i.e., that the selected genotypes are rare in the ancestral population), since somatic cells do not recombine during growth and the population size is not small (N = approximately 10^4 cells), we can employ deterministic selection theory applied

to competing clones to infer the approximate initial frequency and fitness advantage of the positively-selected genotypes (*17*). After t generations, the frequency of a focal clone, p_t, can be calculated from the equation $\frac{p_t}{q_t} = \frac{p_0}{q_0}(w^*)^t$, where $q = 1–p$ represents the frequency of the competing clone(s); p_0 is the initial frequency of the focal clone; and $w*$ is the fitness advantage of the focal clone relative to wild type. The relationship between the initial relative frequency of a clone (p_0), its relative fitness advantage ($w*$), and its expected relative frequency after t generations (p_t) is shown in **Table S1**. Comparison of the experimental values (**Fig. S2**, black squares) with the theoretical predictions revealed that the observations are consistent with a rapid increase in frequency (approximately 20 generations) of an initially rare clone with an approximately twofold selective advantage over the wild type ($w*\approx 2$).

Testing the hypothesis of adaptive evolution on soft substrates with whole exome sequencing and simulations

To investigate the possibility that the observed evolution could be explained simply by random genetic drift, we performed whole exome sequencing in evolved and ancestral populations and conducted simulations of *in silico* experimental evolution for comparison. Evolution is driven by a change in frequency of genetic variants. However, whether the change is detectable over a specific time period will depend on the initial frequencies of the selected variants and the distribution of selection coefficients (*17*). Accordingly, to quantify cell evolution at the genomic level, we analyzed a sample of the ancestral population, a pooled sample of three lines independently evolved on the stiff substrate, and two pooled samples each containing three lines independently evolved on the soft substrate, by whole-exome sequencing at an approximately 1000× median coverage. The distributions of allele frequencies in the four samples are shown in

Fig. 3A. An example of the evolution of allele frequencies on a finer scale is shown in **Fig. 3B**. The distributions of the two sets of pooled soft-evolved lines were very similar, and distinct from those of the pooled stiff-evolved lines and of the ancestral population. When compared to the ancestor (purple curve), the frequency distribution of the soft-evolved lines showed both a small peak of high-frequency variants (black arrow), as expected if some variants were increasing toward fixation, and a larger peak of low-frequency variants (blue arrow), as expected if a large fraction of variants was being removed from the population by selection. The same trend was evident in the stiff-evolved sample, except that the peaks were observed at less extreme frequencies, which was consistent with the directional selection being weaker (and hence the timescale of evolution slower) on the stiff substrate than

on the soft substrate.

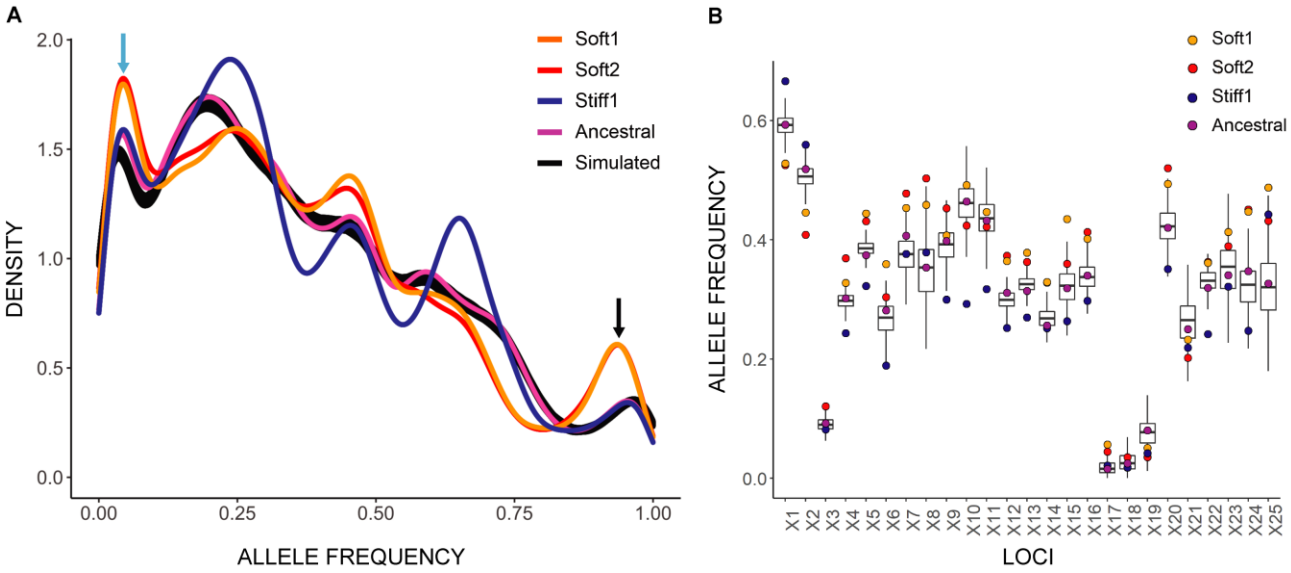

Fig. 3. Density plot of alternative allele frequencies in the ancestral population and evolved lines. (A) Two sets of three randomly chosen soft-selected lines were pooled to form two groups (Soft1 and Soft2). Three lines independently evolved on the stiff substrate were also pooled (Stiff1). Exome sequencing of the pooled lines and ancestral population was performed at 1000×

coverage, and allele frequencies calculated. The two pooled sets of soft-evolved lines exhibited an excess of alleles that were close to fixation or extinction (black and blue arrow). Black line, allele frequencies calculated from 500 simulated trajectories in the absence of natural selection (see text). (B) Change in allele frequency by locus, shown for the first 25 polymorphic loci on Chromosome 1. The boxplots represent the variation from 500 simulations expected in the absence of selection.

Next, to quantify the extent of allele frequency change expected to occur in evolving populations as a result of random sampling (i.e., genetic drift, sample pooling, and sequencing), we simulated the 90 d sustained culture experiment described in **Fig. 2A** forward-in-time in the absence of selection (and mutation). We constructed replicate lines as in the experiments *in silico* by randomly sampling 10^4 completely linked diploid mouse genomes from a starting pool of 6×10^4 genomes (each genome represents one cell) with the allele frequencies sampled with replacement from the observed allele frequency distribution in the ancestral population (purple curve in **Fig. 3A**). This simulated population was allowed to grow and evolve for 90 d, bottlenecking to 10^4 genomes at 3-generation intervals to represent cell passaging at 3 d intervals. Two sets of three pooled lines were sequenced *in-silico* with the coverage mirroring the experimentally observed sequencing coverage at each locus. Over the course of 90 d, the average absolute change in allele frequency ($|\Delta p|$) across 500 simulations was 2.7% (simulation range 2.66% to 2.74%). The observed change in the experimental soft- and stiff-evolved lines was 4.4% and 3.7%, respectively ($P < 0.002$ based on 500 simulations). The average absolute relative change in allele frequency ($|\Delta p|/p$) across 500 simulations was 14.1% (simulation range 13.8% to 14.4%). The observed change in the soft- and stiff-substrate-evolved lines was 21.7% and 18.2%, respectively ($P < 0.002$). Further, 13.7% of sites in the soft-evolved lines and 12.1% sites in the stiff-substrate-evolved lines exceeded the maximum change for the sites across 500 simulations

[the expectation being that 0.2% (1/500) of sites would exceed the maximum; see section 3 in supplemental information]. While this magnitude of allele frequency change is inconsistent with random genetic drift, it is consistent with evolution by natural selection.

Phenotypic evolution on substrates of defined rigidity

Since the cell fitness increased over the course of the experiments (**Fig. 2B**), we next examined the directionality of phenotypic trait adaptation to discriminate between the possibilities depicted in **Fig. 1**. We evaluated three traits that have been previously shown to exhibit plasticity in cells cultured on substrates of different rigidities: cell spreading, Yes-associated protein (YAP) localization in the nucleus (*18*), and cytoskeletal organization (*19*). After 3 months of evolution on the soft substrate, both cell spreading area and nuclear/cytoplasmic ratio of YAP were statistically indistinguishable from the ancestral value on the stiff substrate (**Fig. 4A–D**). By contrast, these traits did not change in cells evolved on the stiff substrate for 3 months. When cultured on soft substrates, ancestral cells did not assemble F-actin structures organized into linear contractile fibers and distinct microtubules, unlike ancestral cells cultured on the stiff substrate (**Fig. 4E**). Following evolution on the soft substrate, the cells gained the ability to assemble distinct F-actin fibers and microtubule networks comparable to cells on the stiff substrates. These results indicate that phenotypes of cells tend to evolve to "revert to normal" on soft substrates (see **Fig. 1**). Again, this phenotypic evolution required genetic variability in the starting population, because it was not observed in clonal cell populations (**Fig. S3**).

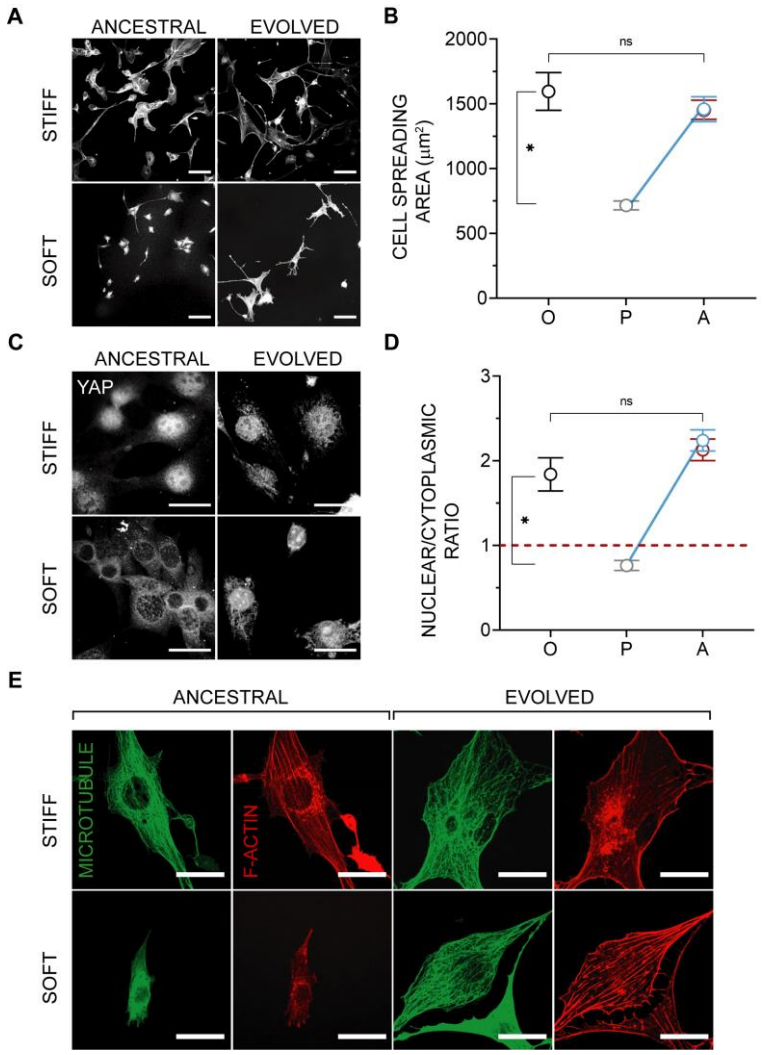

Fig. 4. Directionality of phenotypic trait adaptation. (A) Representative images of F-actin in ancestral populations cultured on the soft or stiff substrate for 3 d, and of selected lines after 90 d of culture on the soft or stiff substrate; scale bar: 100 μm. (B) Mean spreading area of the ancestral cells on stiff substrate (O), ancestral cells on soft substrates (P) and selected lines after sustained culture (A) on soft (blue) or stiff substrates (red) (A); compare with the scheme in Figure 1. Error bars, SEM; each data point represents the mean value from over 50 cells from three lines (randomly chosen); Kruskal-Wallis test with Dunn's multiple comparisons test, *$P < 0.05$; ns, $P > 0.05$. (C) Representative images of YAP in ancestral populations cultured on the soft or stiff substrate for 3

d, and in selected lines after 90 d of culture on the soft or stiff substrate; scale bar: 30 μm. (D) Mean nuclear to cytoplasmic YAP intensity ratio in ancestral cells on stiff substrate (O), ancestral cells on soft substrates (P) and selected lines after sustained culture (A) on soft (blue) or stiff substrates (red) (A); compare with the scheme in Figure 1. Error bars, SEM; each data point represents the mean value from over 50 cells from three lines; Kruskal-Wallis test with Dunn's multiple comparisons test, $*P < 0.05$; ns, $P > 0.05$. (E) F-actin and microtubule structures in ancestral cells and selected lines after sustained culture on soft and stiff gels. Scale bar: 30 μm. (C and E)

The finding that it is possible to select for genetic variants with novel phenotypes suggests that phenotypic plasticity observed on soft and rigid substrates must at least in part be genetically determined. We confirmed this finding through separate experiments in which we asked if the area of cell spreading correlates with the genetic makeup of cells. We isolated nine fibroblast clones, expanded them into clonal lines, and then cultured these clonal cells on soft and stiff substrates. The clonal cells had low areas on soft substrates, and high areas on stiff substrates as expected (**Fig. S4)**. Strikingly, when the areas of the clones on the stiff and soft substrate were plotted against each other, there was a strong correlation (**Fig. S4**). That is, clones that spread less on soft substrates also spread less on stiff substrates and vice versa. As the only difference between the clones is their genetic make-up, these data support the concept that variation among cells in phenotypic plasticity is the result of underlying genetic variation.

Patterns of gene expression

To understand the mechanisms underlying cellular evolution on the soft substrate, we next evaluated gene expression in lines that evolved for 3 months on the soft substrate. These evolved cells were then cultured on the soft or stiff substrates for 3 d, harvested and analyzed by RNA

sequencing. We also evaluated gene expression in the ancestral populations cultured for 3 d on the soft or stiff substrates. We used principal component analysis (PCA) to cluster all samples based on the respective gene expression profiles (**Fig. 5A**). The first two principal components (PCs) explained approximately 80% of the total variance. PC1, which explained approximately 51% of the variance, clearly separated the ancestral and evolved populations. PC2, which explained 28% of the variance, separated the evolved populations into two distinct clusters, but there was no obvious correspondence between the clusters and substrate stiffness. By contrast, clustering of PC2 for a given selected line, independent of the substrate that the cells were cultured on, suggested that the evolved lines evolve distinct patterns of gene expression independent of substrate. Collectively, these observations suggest that different soft-selected lines recovered fitness and potentially evolved the same phenotypic traits via at least two distinct transcriptional architectures.

The "revert to normal" pattern of evolution observed on the soft substrate (**Fig. 4**) is consistent with similar patterns observed in both experimental (*20*) and natural populations (*21*), in which gene expression has been shown to tend to revert to normal. Consequently, we asked whether gene expression also tends to revert to normal upon cellular evolution on the soft substrate. However, there is a known statistical bias for gene expression to apparently revert to normal (reversion) as opposed to becoming even more extreme (reinforcement)(*22*). To account for this potential bias, we used a parametric bootstrap approach(*23*) to analyze all genes that exhibited statistically significant plasticity. This method involves re-sampling from a simulated normal distribution with the mean and variance equal to the observed values for each transcript (see SI Methods). Using the sampled values, we calculated the *PC* (plastic change) and *GC* (genetic change): $PC = L_p - L_o$, where L_o and L_p represent gene expression levels in the original environment (stiff substrate) and upon plastic change (soft substrate); $GC = L_a - L_p$, where L_a represents gene

expression on the soft substrate after evolution. The *GC* to *PC* ratio captures both the magnitude and direction of change in gene expression upon evolution. If the ratio is negative, the gene expression is reverted, and if it is positive, the gene expression is reinforced. The propensity of gene expression levels to revert or reinforce is captured by the parameter δ; $\delta = C_{RV} - C_{RI}$, where C_{RV} is the fraction of reverted genes, while C_{RI} is the fraction of reinforced genes, both at a significance level of $P < 0.05$. We found that δ for the eight lines on the soft substrate was approximately 3.8%. This indicated a minor bias toward reversion.

Next, to determine whether the difference along PC2 in the two clusters is associated with a difference in tendency to revert (RV) or reinforce (RI), we repeated the above analysis separately for the two clusters of evolved populations separated along PC2. For the North cluster, δ_1 = 12.09%, indicating a trend toward reversion; for the South cluster, δ_2 = 2.40% indicating a minor trend toward reversion. To address the possibility that the δ_1–δ_2 difference (9.7%) could be simply a result of sampling variance, we generated a null distribution of $\delta_1 - \delta_2$ by randomly sampling eight replicates from the distributions of *GC* and *PC*, and assigning them arbitrarily to one of two groups. The simulated null distribution is shown in **Fig. 5B**. The observed difference falls well outside the right tail of the distribution (red arrow in **Fig. 5B**), implying that the observed difference cannot be explained by sampling. These observations demonstrate that the separation of the two clusters along PC2 is caused at least in part by the tendency of genes to revert. That is also apparent from the $\langle GC \rangle / \langle PC \rangle$ distributions over all genes that exhibit significant plasticity in the two groups (**Fig. 5C**). Specifically, the distribution is skewed toward negative values (i.e., reversion) for the North cluster, with no such trend in the South cluster. Fig. 5D provides a visual representation of reversion and reinforcement of individual genes which were identified from the parametric bootstrap simulation as significantly reverted or reinforced. Collectively (**Fig. 5B–D**),

these observations indicate that different populations can evolve the same phenotypes by means of qualitatively different transcriptional pathways.

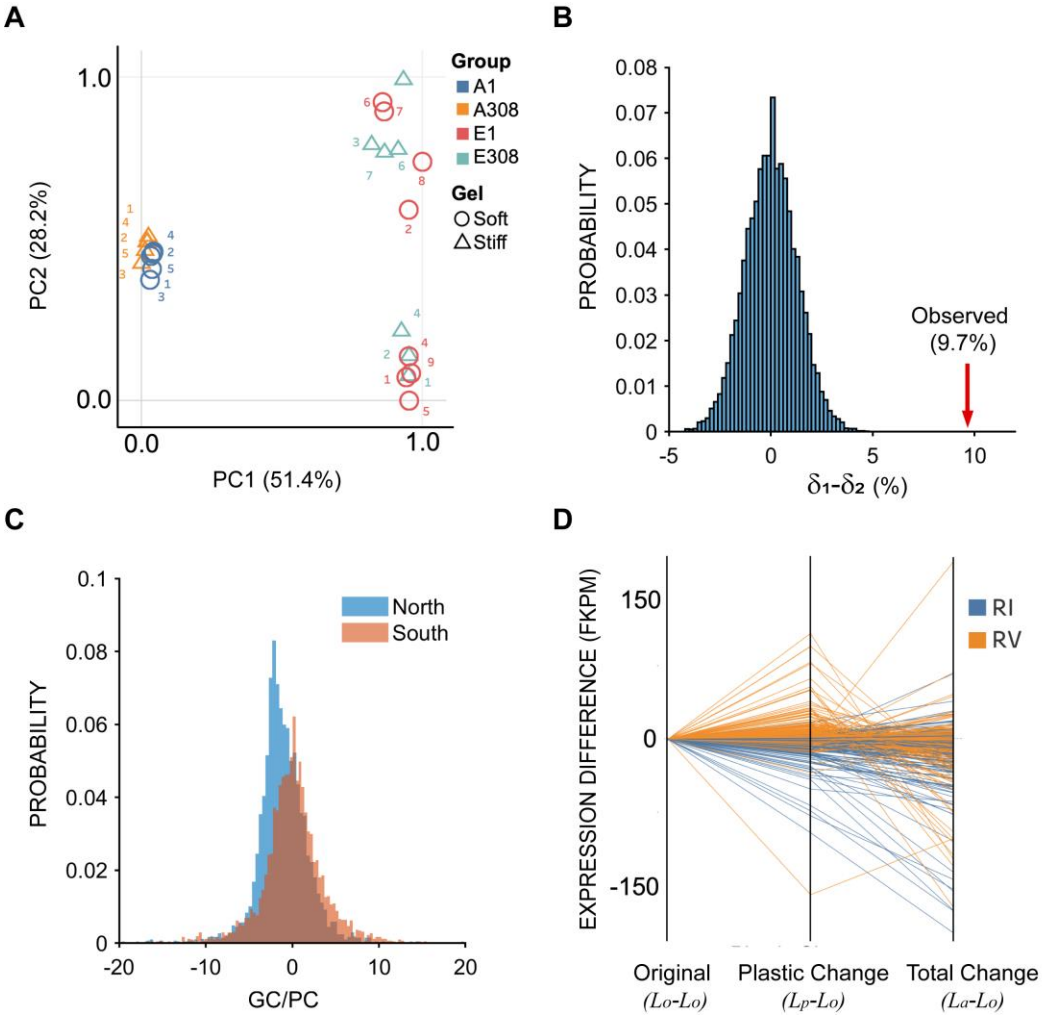

Fig. 5. Analysis of gene expression. (A) Principal component analysis (PCA) of gene expression profiles. A1 and A308 represent ancestral cells cultured for 3 d on the soft (1 kPa) and stiff (308 kPa) substrates respectively. E1 and E308 represent cells evolved for 90 on the soft substrate (1 kPa) followed by 3 d culture on the soft (1 kPa) and stiff substrate (308 kPa) respectively. (B) Null $\delta_1 - \delta_2$ distribution generated by randomly sampling eight replicates from the *GC* and *PC* distributions (see text for definition of *GC* and *PC*). The actual value for $\delta_1 - \delta_2$ is indicated by a red arrow (see text). (C) Probability distributions of <*GC*>/<*PC*> over all genes that exhibited

statistically significant plasticity in the North (top cluster along PC2 in Fig. 5A) and South (bottom cluster along PC2 in Fig. 5A) clusters computed from parametric bootstrap simulations. (D) Parallel coordinate graphs depicting reversion or reinforcement of 449 genes identified as significantly reverted or reinforced from the parametric bootstrap simulation. Orange lines depict reversion (RV), blue lines depict reinforcement (RI); the indicated quantities at the bottom of the x-axis are plotted for each individual, identified gene.

Because δ was significantly different from zero and positive (which indicated a bias for genes to revert) only for the North cluster, we also performed ontology analysis of genes that reverted in the North cluster. These genes were enriched in biological processes related to mitosis and the cell cycle, and included microtubule-chromosome association (kinetochore organization), spindle organization, chromosome segregation, and regulation of cell cycle phases (**Fig. S5**; see supplemental methods). This is consistent with the phenotype returning to normal in terms of the growth rate on the soft substrate upon evolution (**Fig. 2**). It also suggests that the "revert to normal" of cell spreading and YAP nuclear localization likely regulate the expression of genes associated with the growth rate.

Discussion

Although there is a vast body of work on experimental evolution of microbes (*24*), there have been relatively few formal evolution experiments with cultured somatic cells (e.g. (*25*)). Despite the fact that the mechanical environment is a ubiquitous influence on most adhesion-dependent cells, there have been no studies that have examined whether mechanical properties of the microenvironment can exert selection pressure on cellular populations. Here we showed that natural selection imposed by the soft substrate selected for existing low frequency genetic variants in the original population that increased fitness on the novel soft substrate. Cell phenotypic values

and associated gene expression on soft substrates tended to “revert to normal”, that is, they became indistinguishable from the corresponding values on the stiff substrate. These findings lend support to growing recent evidence that not all phenotypic plasticity is inherently adaptive ((*10*) and references therein). It is important to note that these results were not a foregone conclusion. For example, had the lines evolved increased fitness on the soft substrate by (say) evolving even smaller spreading areas ("evolutionary head start"; **Fig. 1**), this would have been consistent with the notion that millions of years of evolution has provided mammalian cells with a plastic repertoire by which the phenotype is close to optimal no matter what the context. Gene expression analysis revealed that different evolved lines achieve similar phenotypic outcomes by means of different underlying transcriptional architectures. This is likely due to the fact that evolution selected for rare variants in the starting population.

Evolution on the soft substrate resulted in a reversion to normal of cell phenotypes like cell spreading, YAP localization in the nucleus and cytoskeletal organization. Such phenotypes are typically sensitive to a wide range of biomaterial properties such as nanostructure, porosity, adhesive ligand presentation, hydrophobicity and biomaterial composition as well as diverse mechanical cues, such as stretch and hydrodynamic shear (*26-34*). We therefore predict that it is feasible for a variety of biomaterial properties and other types of mechanical stimuli to impose natural selection on cells during sustained culture. There are hundreds of somatic cell lines that have been propagated for years or decades that constitute a rich, nearly untapped resource that can be utilized in the context of experimental evolution on biomaterials. An obvious limitation of the experimental approach here from a tissue engineering perspective is that it is not suited for primary cells that lack genetic variability or that cannot be passaged for long times. However, an attractive aspect of experimental evolution with genetically variable cell lines is that it could help reveal

specific alleles underlying increased fitness of the evolved populations, and identify novel molecular mechanisms underlying cellular sensing of diverse biomaterial properties. Such knowledge could then make it possible to perform targeted genetic engineering of primary cells with CRISPR or other methods to promote desired phenotypes on biomaterials of one's choice. Also, given that mechanical properties of the extracellular matrix are crucially important in cancer progression (e.g. (*35*, *36*)), we predict that experimental evolution may especially important in understanding the mechanical underpinnings of cancer.

References and Notes

1. C. F. Guimarães, L. Gasperini, A. P. Marques, R. L. Reis, The stiffness of living tissues and its implications for tissue engineering. *Nature Reviews Materials*, (2020).
2. D. E. Discher, P. Janmey, Y. L. Wang, Tissue cells feel and respond to the stiffness of their substrate. *Science* **310**, 1139-1143 (2005).
3. A. J. Engler, S. Sen, H. L. Sweeney, D. E. Discher, Matrix elasticity directs stem cell lineage specification. *Cell* **126**, 677-689 (2006).
4. V. M. Weaver, Cell and tissue mechanics: the new cell biology frontier. *Mol Biol Cell* **28**, 1815-1818 (2017).
5. N. Shakiba, P. W. Zandstra, Engineering cell fitness: lessons for regenerative medicine. *Curr Opin Biotechnol* **47**, 7-15 (2017).
6. A. R. Killaars *et al.*, Extended Exposure to Stiff Microenvironments Leads to Persistent Chromatin Remodeling in Human Mesenchymal Stem Cells. *Adv Sci (Weinh)* **6**, 1801483 (2019).
7. C. X. Li *et al.*, MicroRNA-21 preserves the fibrotic mechanical memory of mesenchymal stem cells. *Nat Mater* **16**, 379-389 (2017).
8. C. Yang, M. W. Tibbitt, L. Basta, K. S. Anseth, Mechanical memory and dosing influence stem cell fate. *Nat Mater* **13**, 645-652 (2014).
9. T. D. Price, A. Qvarnstrom, D. E. Irwin, The role of phenotypic plasticity in driving genetic evolution. *Proc Biol Sci* **270**, 1433-1440 (2003).
10. W. C. Ho, J. Zhang, Evolutionary adaptations to new environments generally reverse plastic phenotypic changes. *Nat Commun* **9**, 350 (2018).
11. C. M. Lo, H. B. Wang, M. Dembo, Y. L. Wang, Cell movement is guided by the rigidity of the substrate. *Biophys J* **79**, 144-152 (2000).
12. S. Munevar, Y. L. Wang, M. Dembo, Distinct roles of frontal and rear cell-substrate adhesions in fibroblast migration. *Mol Biol Cell* **12**, 3947-3954 (2001).
13. H. B. Wang, M. Dembo, S. K. Hanks, Y. Wang, Focal adhesion kinase is involved in mechanosensing during fibroblast migration. *Proc Natl Acad Sci U S A* **98**, 11295-11300 (2001).
14. R. J. Pelham, Jr., Y. Wang, Cell locomotion and focal adhesions are regulated by substrate flexibility. *Proc Natl Acad Sci U S A* **94**, 13661-13665 (1997).
15. D. B. Lovett, N. Shekhar, J. A. Nickerson, K. J. Roux, T. P. Lele, Modulation of Nuclear Shape by Substrate Rigidity. *Cell Mol Bioeng* **6**, 230-238 (2013).
16. J. D. Mih *et al.*, A multiwell platform for studying stiffness-dependent cell biology. *PLoS One* **6**, e19929 (2011).
17. J. B. S. Haldane, A mathematical theory of natural and artificial selection, Part V: Selection and mutation. . *Proceedings of the Cambridge Philosophical Society*. **23:838-44**, (1927).
18. S. Dupont *et al.*, Role of YAP/TAZ in mechanotransduction. *Nature* **474**, 179-183 (2011).
19. C. E. Chan, D. J. Odde, Traction dynamics of filopodia on compliant substrates. *Science* **322**, 1687-1691 (2008).
20. S. S. Fong, A. R. Joyce, B. O. Palsson, Parallel adaptive evolution cultures of Escherichia coli lead to convergent growth phenotypes with different gene expression states. *Genome Res* **15**, 1365-1372 (2005).
21. C. K. Ghalambor *et al.*, Non-adaptive plasticity potentiates rapid adaptive evolution of gene expression in nature. *Nature* **525**, 372-375 (2015).

22. F. Mallard, A. M. Jaksic, C. Schlotterer, Contesting the evidence for non-adaptive plasticity. *Nature* **555**, E21-E22 (2018).
23. W. C. Ho, J. Zhang, Genetic Gene Expression Changes during Environmental Adaptations Tend to Reverse Plastic Changes Even after the Correction for Statistical Nonindependence. *Mol Biol Evol* **36**, 604-612 (2019).
24. R. E. Lenski *et al.*, Sustained fitness gains and variability in fitness trajectories in the long-term evolution experiment with *Escherichia coli*. *Proceedings of the Royal Society B-Biological Sciences* **282**, (2015).
25. T. B. Taylor, A. V. Wass, L. J. Johnson, P. Dash, Resource competition promotes tumour expansion in experimentally evolved cancer. *Bmc Evolutionary Biology* **17**, (2017).
26. L. Li, J. Eyckmans, C. S. Chen, Designer biomaterials for mechanobiology. *Nat Mater* **16**, 1164-1168 (2017).
27. G. Brusatin, T. Panciera, A. Gandin, A. Citron, S. Piccolo, Biomaterials and engineered microenvironments to control YAP/TAZ-dependent cell behaviour. *Nat Mater* **17**, 1063-1075 (2018).
28. S. Kumar, K. Chatterjee, Comprehensive Review on the Use of Graphene-Based Substrates for Regenerative Medicine and Biomedical Devices. *ACS Appl Mater Interfaces* **8**, 26431-26457 (2016).
29. S. Chien, Mechanotransduction and endothelial cell homeostasis: the wisdom of the cell. *Am J Physiol Heart Circ Physiol* **292**, H1209-1224 (2007).
30. S. N. Bhatia, D. E. Ingber, Microfluidic organs-on-chips. *Nat Biotechnol* **32**, 760-772 (2014).
31. P. Zorlutuna *et al.*, Microfabricated biomaterials for engineering 3D tissues. *Adv Mater* **24**, 1782-1804 (2012).
32. B. R. Freedman, D. J. Mooney, Biomaterials to Mimic and Heal Connective Tissues. *Adv Mater* **31**, e1806695 (2019).
33. D. Huber, A. Oskooei, I. S. X. Casadevall, d. Andrew, G. V. Kaigala, Hydrodynamics in Cell Studies. *Chem Rev* **118**, 2042-2079 (2018).
34. T. Iskratsch, H. Wolfenson, M. P. Sheetz, Appreciating force and shape-the rise of mechanotransduction in cell biology. *Nat Rev Mol Cell Biol* **15**, 825-833 (2014).
35. J. J. Northey, L. Przybyla, V. M. Weaver, Tissue Force Programs Cell Fate and Tumor Aggression. *Cancer Discov* **7**, 1224-1237 (2017).
36. M. C. Lampi, C. A. Reinhart-King, Targeting extracellular matrix stiffness to attenuate disease: From molecular mechanisms to clinical trials. *Sci Transl Med* **10**, (2018).

Supplementary Information:

Materials and Methods:

1. **Experimental cell evolution on soft and stiff substrates**

Synthesis and functionalization of hydrogels

Polyacrylamide gels of different stiffness were prepared by using a well-established protocol (*1*). Acrylamide and bis-acrylamide (Bio-rad) were mixed in 50:1 and 12.5:1 ratios to prepare gels with Young's modulus (*E*) of 1 kPa and 308 kPa, respectively, as previously described (*2*). We have previously shown that the cells sense gel stiffness in this assay and not other properties like ligand spacing (*2*). The gel solutions contained 99.4% v/v gel mixture, 0.5% v/v ammonium persulphate (ThermoFisher Scientific), and 0.1% v/v tetramethylethylenediamine (ThermoFisher Scientific). For each gel, 100 μl of the gel solution was sandwiched between a hydrophobic glass surface and a hydrophilic glass coverslip (18 mm in diameter) for 20 min. The gels were functionalized using sulfosuccinimidyl 6-(4'-azido-2'-nitophenylamino) hexanoate (G Biosciences) and coated with fibronectin (10 μg/ml) before cell seeding.

Cell culture

The mouse fibroblast cell line NIH 3T3 and the mouse myoblast cell line C2C12 were purchased from the American Type Culture Collection. Both cell lines have been cultured for decades on (stiff) tissue culture plastic, and are expected to be at or near genetic equilibrium. The cells were cultured in 89% Dulbecco's modified Eagle's medium with 4.5 g/l glucose, 4 mM L-glutamine, and 1 mM sodium pyruvate (Corning Inc.), supplemented with 10% donor bovine serum (Gibco) and 1% penicillin-streptomycin mix (Corning Inc.). The cultures were maintained at 37 °C in a humidifier, under 7% CO_2. The cells were detached from tissue culture dishes or gel surfaces using 0.25% trypsin (Corning Inc.) when the culture reached 70–80% confluence and were seeded onto new dishes/gels.

Cloning

NIH 3T3 fibroblasts were seeded on a dish (10 cm in diameter) at a density of 500 cells/ 10 cm diameter dish and were allowed to grow for 5–7 d. At that time, the cells formed 5–10 distinct colonies separate from one other. Each colony was isolated by placing a glass cloning ring (8 mm in diameter) on the surface of the tissue culture dish that enclosed a colony and trypsinizing the area of the dish enclosed by the cloning ring (*3*). The colonies were then grown independently in separate tissue culture dishes to obtain clones.

Growth rate measurements

Lines propagated on a given substrate were sampled at specific time points for growth rate measurements. Cells were trypsinized from the substrate of a given stiffness, a fixed number of cells were seeded on another substrate of the same stiffness, and allowed to grow for 3 d. On day 3, the cells were trypsinized from the gel surface. The trypsinized cells were suspended in 1 ml of the cell culture medium. Then, 10 μl of cell suspension was pipetted and mixed with 0.4% trypan blue (ThermoFisher Scientific) in 1:1 ratio. The cells were counted using Countess II Automated Cell Counter (ThermoFisher Scientific). The total live cell count/ml was recorded as the final number of cells and the growth rate was calculated as $N_f = N_0\, 2^{\eta t}$, where N_f is the final cell count; N_0 is the initial cell count which was determined by the same procedure before seeding and was fixed at 10,000 cells; t is time (3 d); and η is the growth rate (per d).

Immunofluorescence staining and microscopy

Cells grown on the soft and stiff gels were fixed in 4% (wt/vol) paraformaldehyde (Alfa-aesar) in water, permeabilized with 0.2% Triton X-100 (Sigma) in PBS, and blocked with 1 mg/ml of bovine serum albumin (Sigma). Primary antibodies toward tubulin or YAP were added, and samples were incubated overnight at 4 °C. Subsequently, the samples were incubated with secondary antibodies for 2 h at room temperature. Microtubules were labeled using rabbit polyclonal anti-alpha tubulin antibody (ab18251; Abcam; dilution 1:600); and YAP was labeled using mouse monoclonal anti-YAP antibody (sc-271134; Santa Cruz Biotechnology; dilution 1:250). The secondary antibodies used were Alexa fluor 488-conjugated goat anti-rabbit antibody (A11008; Invitrogen; dilution 1:1000) and Alexa fluor 594-conjugated goat anti-mouse antibody (A11005; Invitrogen; dilution 1:1000). Nuclei were stained using Hoechst 33342 (Life Technologies) and F-actin was stained using Alexa fluor 647-conjugated phalloidin (A22287, Invitrogen). The gels were mounted on fluoro-dishes using ProLong Gold Antifade Mountant (ThermoFisher Scientific). Samples were imaged using a Nikon A1+ confocal microscope equipped with DU4 detector, and 20× air or 60× 1.4 NA oil-immersion objectives. Images were acquired using the NIS Elements 5.02 software (Nikon).

Cell area analysis

For cell area measurements, bright field images of cells attached to the gels were acquired using Zoe Fluorescent Cell Imager (BioRad); images of F-actin (following phalloidin staining in cells) were acquired using 20× objective on a Nikon A1+ confocal microscope. Images were acquired at different locations on the gel surface and the area of each cell was determined using ImageJ software.

Measurement of the nuclear to cytoplasmic YAP ratio

The nuclear and cytoplasmic intensity of YAP was measured using ImageJ software. The nuclear boundary was traced in the fluorescent image, and the average YAP intensity in that area was measured using an ImageJ tool. The cytoplasmic intensity and background intensity were similarly determined by tracing areas. The nuclear to cytoplasmic YAP ratio was calculated as: [(Nuclear YAP intensity) – (Background intensity)] / [(Cytoplasmic intensity) – (Background intensity)].

Statistical analysis

The normality of distributions of the measured values was tested using the likelihood ratio test. The majority of distributions were not normal. Therefore, statistical comparisons between the control and treatment samples were done using the non-parametric Mann Whitney U test (Fig. 2B, 2C and Fig. S1). For multiple comparisons, Kruskal-Wallis test with Dunn's multiple comparisons test was used (Fig. 2D, 4A, 4C). Graphical plots were generated using Prism version 8.4.0 (GraphPad) , MATLAB version R2019b (Mathworks), and RStudio version 1.1.463 (RStudio Inc.). PCA data visualization (Fig. 5A, 5D) was done using R version 2.12.0 and Tableau Desktop version 2020.1. The details of experimental conditions and statistical tests are provided in figure legends.

The C2C12 growth rate data were analyzed by using the general linear model (GLM) implemented in the MIXED procedure of SAS version 9.4. The GLM can be written as

$$y_{ijk} = \mu + a_i + b_j + c_{ixj} + \varepsilon_{k(i)},$$

where y_{ijk} is the measured growth rate of a sample; μ is the overall mean; a_i is the continuous, linear effect of assay day i; b_j is the fixed effect of substrate j; c_{ixj} is the effect of the interaction between the assay day and substrate; and $\varepsilon_{k(ij)}$ is the residual effect. Variance components were determined using the restricted maximum likelihood method. The significance of fixed effects (day, substrate) was evaluated by F-test using Type III sums of squares. Degrees of freedom were determined by the method of Kenward and Roger (*4*). The linear regression of growth rate on assay day was then calculated separately for each substrate, using the linear model $y_{ij} = \mu + \beta t_j + \varepsilon_{ij}$, where y_{ij} is the growth rate of a sample; μ is the intercept and β is the slope of the linear regression of growth rate on assay day t; and ε_{ij} is the residual effect.

2. Whole-exome sequencing and analysis of gene expression in evolved lines

Whole-exome sequencing (WES) and variant analysis

To quantify evolution at the genomic level, WES (approximately 1000× median coverage) was used to analyze a sample of the ancestral population, a pooled sample containing three fibroblast lines independently evolved for 90 days on the stiff substrate (308 kPa), and two pooled samples each containing three lines independently evolved for 90 days on the soft substrate (1 kPa). Whole exome was captured and sequenced using the Roche SeqCap® EZ MedExome Kit and Illumina NovaSeq® 6000 Sequencer, respectively. To minimize sequencing errors, a sequencing protocol involving unique molecular identifiers was used (*5*) (xGen® Dual Index UMI Adapters from Integrated DNA Technologies). Sequencing reads from each sample were mapped to a mouse reference genome version mm9 using BWA-MEM (*6*). Library preparation, sequencing, de-multiplexing, read alignment, and quality check were performed according the standard laboratory protocols at the University of South California Genomics Core Facility. FreeBayes version 1.2.0 (*7*) joint variant calling method was used to deduce single-nucleotide variants, and small insertions and deletions in the aligned sequencing reads, yielding 750,873 variants. To maximize the capture of low-allele frequencies in the population, the following FreeBayes parameters were used: --pooled-continuous, --pooled-discrete, --min-alternate-fraction 0.001, --min-alternate-count 2, and --allele-balance-priors-off.

RNA extraction, library preparation, and sequencing

Five replicates of the ancestral population and 10 lines of fibroblasts evolved on soft 1 kPa gels for 90 d were each cultured on the soft or stiff gels for 3 d. After 3 d, each replicate population was trypsinized, centrifuged at 250 × *g* for 5 min, and counted to obtain at least 10^6 cells per sample. Approximately 10^6 cells were resuspended in RNAase-free PBS. The suspension was again centrifuged at 1400 × *g* for 3 min, the obtained pellet was flash-frozen in liquid nitrogen and immediately stored at –80 °C. The samples were shipped on dry ice to Novogene Corporation Inc.(Sacramento, California, USA) for RNA extraction and sequencing. There, the cell pellets were resuspended in RLT buffer supplemented with β-mercaptoethanol, lysed using lysis beads (*8*) and total RNA was extracted from the cell lysates using Qiagen RNAeasy mini kit according to the manufacturer's protocol. The quality control of total extracted RNA was performed as follows: (1) preliminary quantitation using NanoDrop (ThermoFisher Scientific); (2) evaluation of contamination and RNA degradation by agarose gel electrophoresis; and (3) RNA integrity analysis using Agilent 2100 analyzer (Applied Biosystems). Samples containing over 0.8 μg of

total RNA and with RNA integrity number > 7.0 were sequenced. Polyadenylated RNA was isolated using oligo(dT) beads. It was then randomly fragmented in a fragmentation buffer using enzyme method, and cDNA was synthesized using random hexamers and reverse transcriptase (included in the NEB Next® Ultra™ RNA Library Prep Kit for Illumina). After the first-strand synthesis, the second strand was synthesized using nick-translation in a customized second-strand synthesis buffer (Illumina) containing dNTPs, RNase H, and *Escherichia coli* polymerase I. The cDNA library was purified, and underwent terminal repair, A-tailing, ligation, size selection, and PCR enrichment, using NEB Next® Ultra™ RNA Library Prep Kit for Illumina (New England BioLabs). Library concentration was determined using Qubit 2.0 fluorometer (Life Technologies); the library was then diluted to 1 ng/μl, and insert sizes were checked using Agilent 2100 analyzer followed by quantitative PCR (Q-PCR) for quantifying to a higher accuracy(library activity>2nM) . Paired-end 150-bp (PE150) sequencing (20 million raw reads) was performed using an Illumina HiSeq sequencer.

RNA sequencing and raw data analysis

Reads with adaptor contamination were trimmed and short reads (< 30 bp) were removed using Trimmomatic (*9*). Cleaned reads were mapped to the mouse genome (version mm9) via HISAT2 (version 2.1.0) (*10*). The counts of aligned reads at the gene level were calculated using featureCounts (Subread version 1.6.2) (*11*) corresponding to the *Mus musculus* Ensembl 67 gene annotations. Weakly expressed genes were removed by retaining only the genes with at least 0.5 counts per million (CPM) in at least one sample. After the filtering step, 15,250 genes out of 35,275 genes remained, and were used in subsequent analysis.

For sample clustering and PCA analysis, counts data were transformed using the regularized log (rlog) method. PCA analysis and data visualization were performed in R using the pcaExplorer package (version 2.12.0) (*12*) based on the top-1000 most variable genes across all samples.

Expression differences between ancestral cells cultured for 3 d on soft substrate (A1) or stiff substrate (A308), and cells pre-evolved on the soft substrate for 90 d and post cultured for 3 d on soft (E1) or stiff substrates (E308) were analyzed by using DEBrowser (version 1.14, DE method: DEseq2, test type Wald) (*13*). Adjusted *P*-value < 0.05 served as a cut-off to determine differentially expressed genes. Differential gene expression was visualized using iDEP.90 (*14*).

Functional categories over-represented in different subsets of genes were determined using WebGestalt 2019 (*15*) with the following parameters: enrichment method, over-representation analysis; minimum number of genes in a category, 20; FDR method, Bonferroni. Non-redundant GO biological processes with FDR < 0.05 are reported.

Parametric bootstrapping

Parametric bootstrapping was done as described elsewhere (*16*). For each transcript, random numbers were drawn from an assumed normal distribution with the observed mean and standard deviation calculated from the RNA sequencing data. Means and standard deviations were calculated for each transcript in the ancestral lines on the stiff and soft substrates, and in cells evolved on the soft substrate. Using these sampled values, *PC* (plastic change) and *GC* (genetic change) were calculated; $PC = L_p - L_o$, where L_o and L_p represent gene expression levels in the original environment (stiff substrate) and upon plastic change (soft substrate), respectively; $GC = L_a - L_p$, where L_a represents gene expression on the soft substrate after evolution. These calculations were repeated 10000 times for every transcript. If more than 9500 events of reversion,

i.e., a change in sign from *GC* to *PC*, occurred, the transcript was classified as reverted. If the signs were the same, it was classified as reinforced. C_{RV} was calculated as the fraction of genes that reverted, while C_{RI} was calculated as the fraction of genes that reinforced.

3. Forward-in-time simulations of experimental evolution

Evolution in a finite population is inevitable because of the random sampling of genomes, i.e., the genetic drift. Sampling variance in the sequencing coverage among loci and among samples will also lead to observed allele-frequency change. To establish the magnitude of allele-frequency change (Δp) consistent with the cumulative effect of genetic drift and sampling of genomes during sequencing of the experimental populations, forward-in-time simulations of *in silico* populations were implemented with the same expected initial allele frequency spectra and demography as those of the actual experimental populations. The following genomic variants (see section on WES above) were excluded from analysis: 1. Those variants whose observed frequencies were consistently over 99% or under 1% across all samples, and 2. Those variants whose "Qual" score was less than 30. This resulted in 42,004 polymorphic genetic variants that were included in the simulation study.

The mouse cells studied here are diploid and genomes do not recombine. Each line was initiated by randomly sampling 10,000 cells (= 20K haploid genomes) from a pool of 60,000 cells with an allele frequency spectrum equivalent to that of the ancestral experimental population (see section on WES above). At each variable site in each simulated (haploid) genome, the allele was assigned with an expectation equal to the observed frequency p_0. The sampling protocol in effect assumes that genomes are initially in linkage equilibrium, which is not true. However, because variable sites are sparse relative to the read length and because individual cells were not sequenced in the current study, the initial haplotype structure was not known. Neutral allele-frequency dynamics at individual loci do not depend on the assumption of linkage equilibrium.

Subsequent to initiation, each population of 10,000 cells went through three cycles of cell division, with the assumption that every cell divides (i.e., there is no cell death), to a confluent population size of 80,000 cells. This mimics the seeding densities and expected division rates of cells in the evolution experiment of Fig. 2A. Haploid genomes were paired in cells, and pairs of genomes doubled with each cell division event. From this population of 80,000 cells, 10,000 cells were randomly drawn without replacement for the next round of population growth, mimicking the passage of cells in the experiment at regular intervals (Fig. 2A). This sampling process was repeated for 26 cycles, nearly equivalent to $N = 78$ cycles of cell growth in the actual experiment. At the terminal generation, lines were randomly pooled into three "pool-seq" sets of three replicates to mimic the experimental exome sequencing approach. The allele-frequency, p', was calculated from the entire sample of 60,000 alleles after sampling the corresponding number of reads for each locus.

The observed difference in allele frequency, $p' - p_0$, is an unbiased estimate of the change in allele frequency, Δp, but it underestimates the sampling variance in Δp because the observed allele frequency in the ancestor is an estimate rather than a known parameter. To re-estimate p' after accounting for the additional sampling variance associated with the estimation of p_0, we generated a sample of n binomially sampled alleles using p' (as the probability of success), where n is the observed coverage at the locus in the ancestor. We call the mean of the n sampled

alleles p^*, and the variance in p^* accounts for all sources of sampling variance: sequencing variance of the ancestor; random genetic drift over the course of the experiment; variation associated with the pooling of replicates of evolved populations; and sequencing variance of the pooled evolved lines. The simulation process was repeated 500 times.

Because the loci are completely linked, the upper bound of the uncorrected *P*-value of an observed Δp greater than the most extreme simulated value is 1/500, and the lower boundary is the inverse of the product of the number of variable sites (N = 42,004) and the number of simulations, i.e., 1/(500*N).

Supplementary Figures:

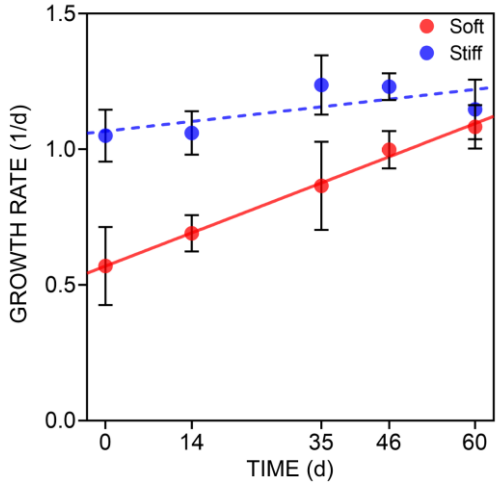

Fig. S1. Measurements of growth rates in C2C12 myoblasts. The mean growth rate of ancestral C2C12 myoblast cell populations on the soft and stiff substrates (1 kPa and 308 kPa respectively) was measured at different times during sustained culture over a 60-d period. Error bars, SEM; data were collected from five or more lines on the soft substrate, and six lines on the stiff substrate at each time point. Statistical significance of the overall trend was determined by GLM (see SI Methods). The lines represent the linear regression of growth rate in time (d). For the growth on the soft substrate (red continuous line; $P < 0.001$), slope = 0.008767 and y-intercept = 0.5694; for the growth on the stiff substrate (blue dashed line; $P > 0.18$), slope = 0.002566 and y-intercept = 1.067. GLM analysis revealed a significant linear increase in growth rate on the soft substrate, but no increasing trend in growth rate on the stiff substrate, as indicated by the significant *day* × *substrate* interaction in the linear model ($F_{1,50.2} = 4.69$, $P < 0.04$). The growth rate increased by approximately 0.88%/d on the soft substrate ($F_{1,25} = 16.24$, $P < 0.001$), whereas there was no significant change in the growth rate on the stiff substrate ($F_{1,27} = 1.87$, $P > 0.18$).

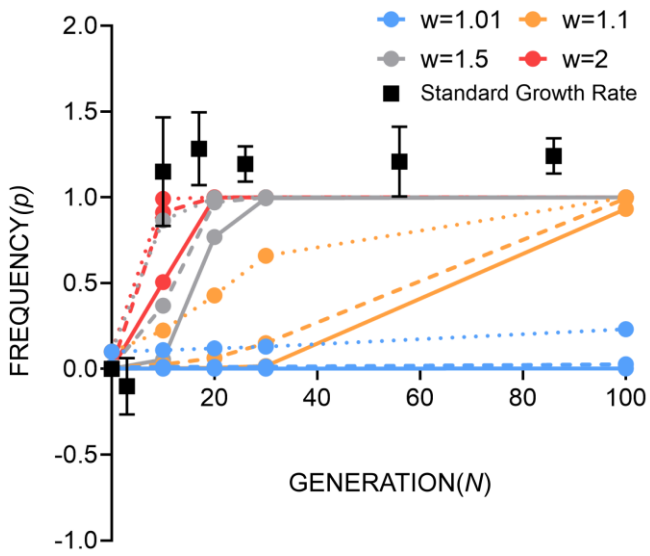

Fig. S2. Fitness advantage of the focal clone relative to wild type. The colored lines depict deterministic clone frequency dynamics from a given starting frequency p_0, with a given strength of selection w, representing the relative fitness of the focal clone relative to the population mean. Solid lines, $p_0 = 0.001$; dashed lines, $p_0 = 0.01$; and dotted lines, $p_0 = 0.1$. Colors denote the strength of selection, as defined in the figure key. Black squares represent the experimentally measured mean growth rate of selected fibroblast lines on the soft substrate (1 kPa) relative to the ancestor (note that the growth rate at generation 3 is lower than the ancestral value); errors bars are S.E.M. Ancestral value was scaled to 0; a value of 1 represents a 100% increase in growth rate.

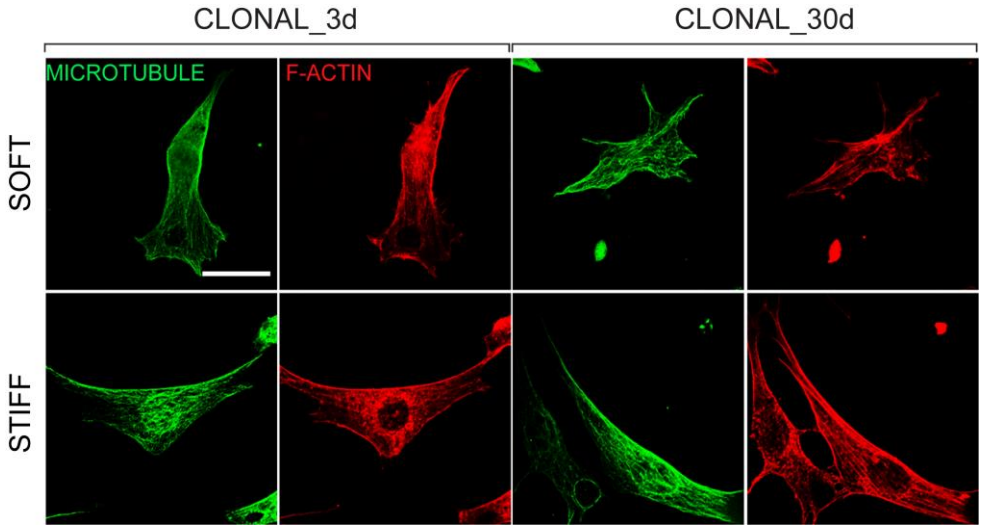

Fig. S3. Cytoskeletal organization in clonal fibroblasts on the soft substrate. Microtubule and F-actin structures in clonal fibroblasts before and after 30 d of sustained culture on the soft and stiff substrates. Scale bar: 30 μm. The cells were immunostained (see methods) and imaged with a 60x objective on a Nikon A1+ confocal microscope. The images are representative of over 100 cells of at least three clonal populations.

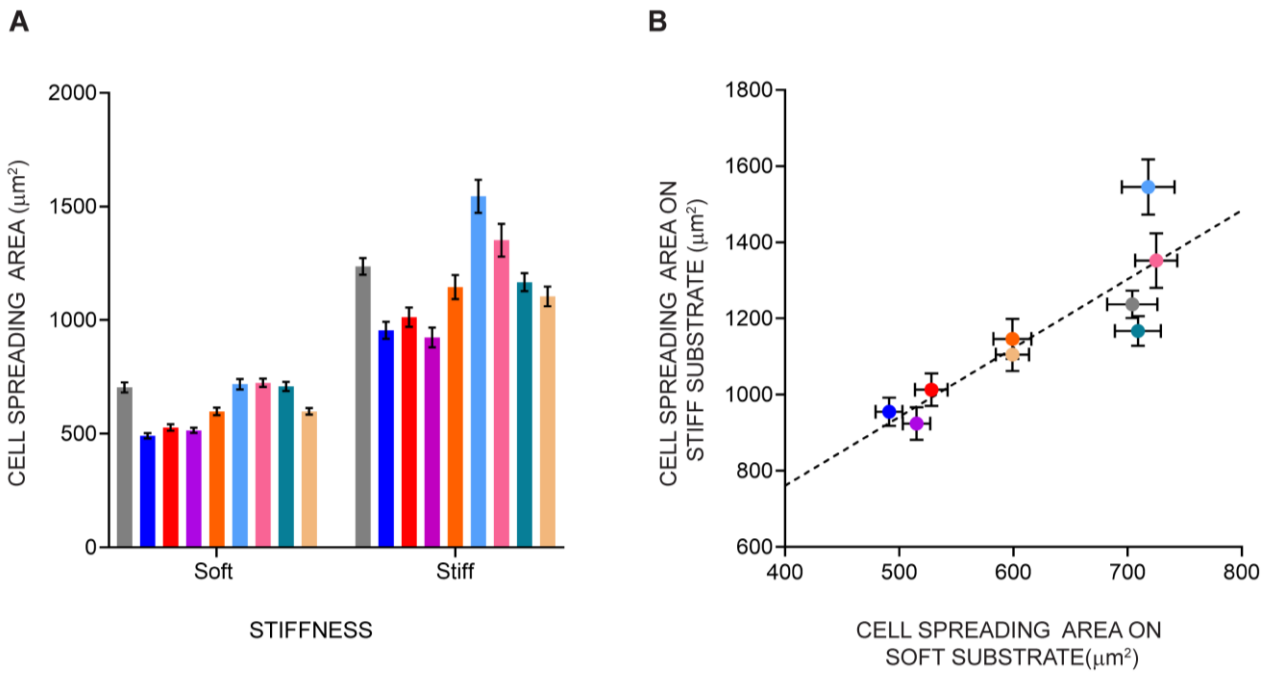

Fig. S4. Area of cell spreading of clonal populations on soft and stiff substrates. (A) Mean area of cell spreading of nine distinct clonal populations, each cultured on soft (1 kPa) or stiff (308 kPa) substrate for 3 d. Error bars, SEM; mean was calculated from at least 140 different cells from three different gels of a given stiffness for each clone. Each color represents an individual clone; this color is the same for a given clone on gels of either stiffness. (B) Mean spreading area of clonal populations from A) on stiff and soft substrates re-plotted against each other. Error bars are S.E.M. The color scheme is the same as in A. Pearson correlation coefficient, $r = 0.87$.

A.

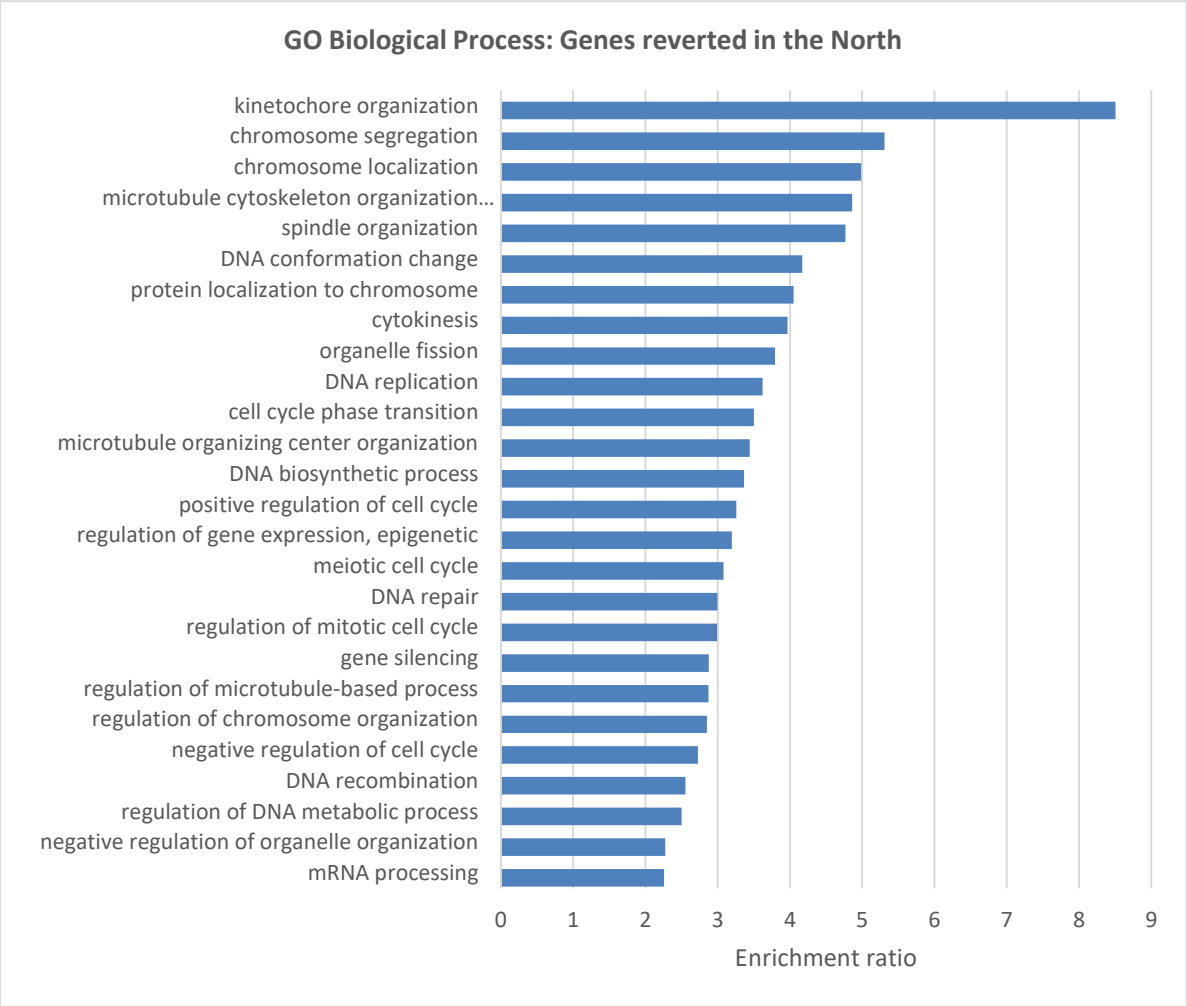
GO Biological Process: Genes reverted in the North
kinetochore organization
chromosome segregation
chromosome localization
microtubule cytoskeleton organization...
spindle organization
DNA conformation change
protein localization to chromosome
cytokinesis
organelle fission
DNA replication
cell cycle phase transition
microtubule organizing center organization
DNA biosynthetic process
positive regulation of cell cycle
regulation of gene expression, epigenetic
meiotic cell cycle
DNA repair
regulation of mitotic cell cycle
gene silencing
regulation of microtubule-based process
regulation of chromosome organization
negative regulation of cell cycle
DNA recombination
regulation of DNA metabolic process
negative regulation of organelle organization
mRNA processing
0
1
2
3
4
5
6
7
8
9
Enrichment ratio

B.

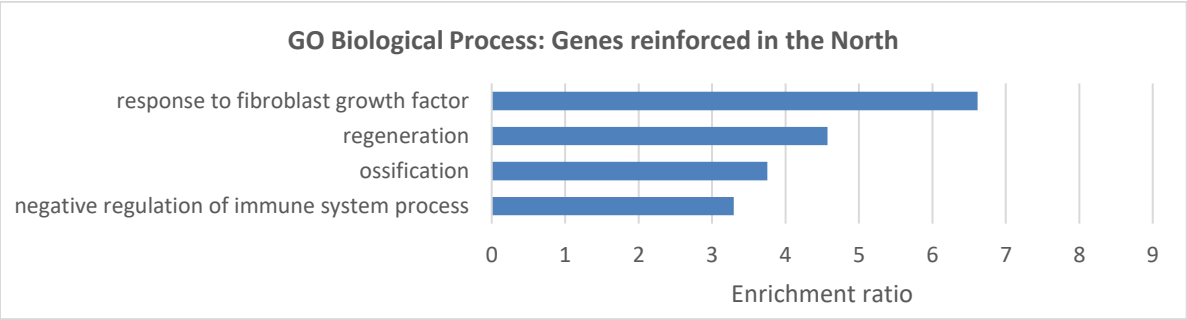
GO Biological Process: Genes reinforced in the North
response to fibroblast growth factor
regeneration
ossification
negative regulation of immune system process
0
1
2
3
4
5
6
7
8
9
Enrichment ratio

C.

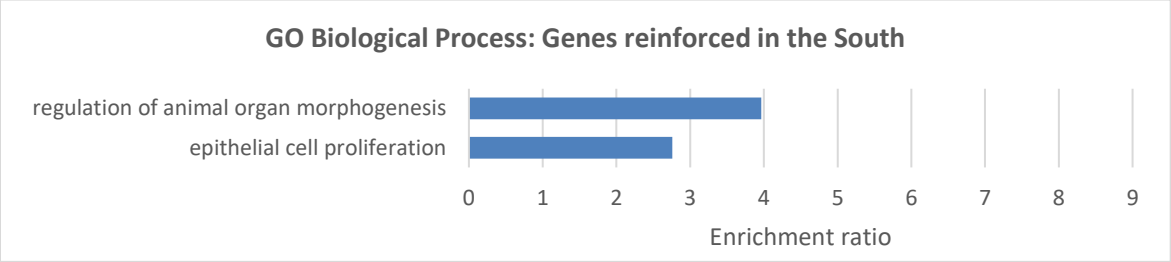

D.

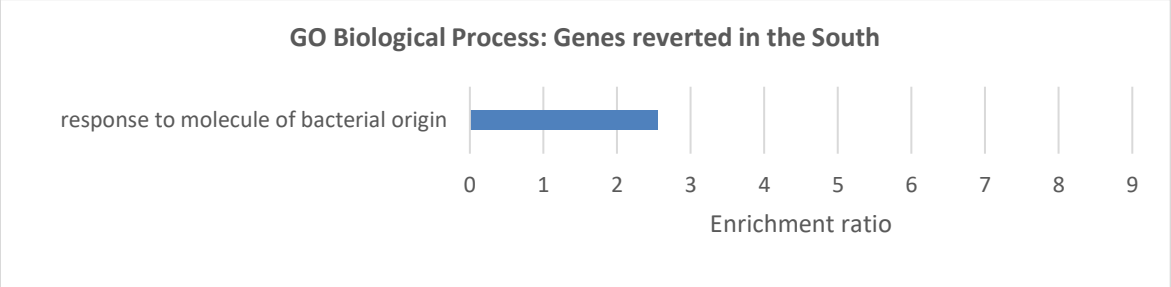

E.

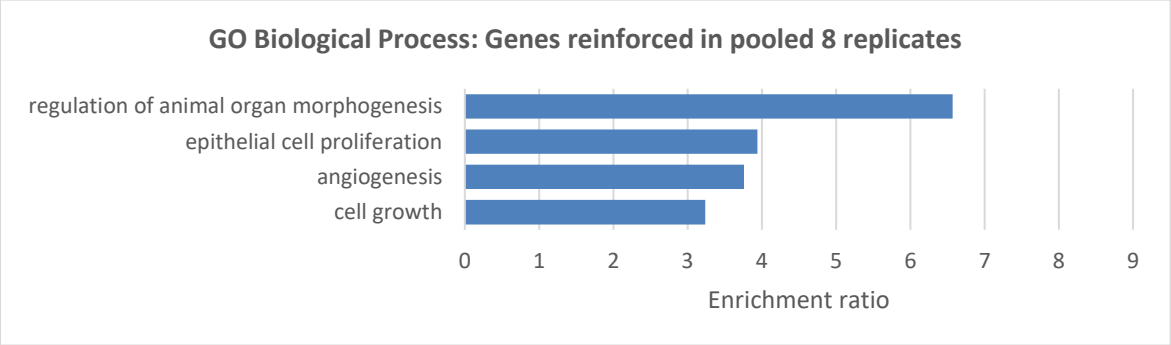

F.

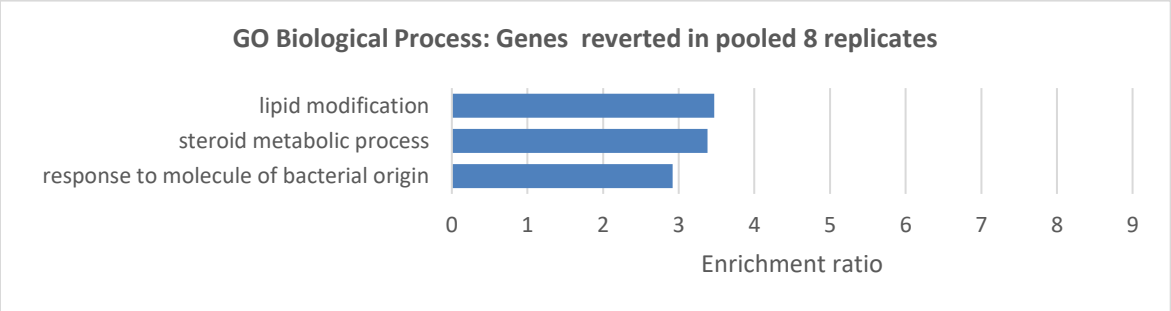

Fig. S5. Gene ontology analysis of the reverted and reinforced genes. The results of over-representation analysis to determine over-represented gene categories identified by parametric bootstrap simulations as reverted or reinforced. Comparisons were made between the gene set of interest and the reference transcriptome (Mus musculus genome protein coding). Results are

shown for the North cluster (A and B; see Fig. 5A for nomenclature), South cluster (C and D), and all pooled samples (E and F; eight replicates evolved on the soft substrate).

Supplementary Table:

p0	w^*/w_{wt}	*p10*	*p30*	*p100*	*p300*
0.0001	1.01	0.000	0.000	0.000	0.002
	1.05	0.000	0.000	0.013	0.996
	1.1	0.000	0.002	0.580	1
	1.25	0.001	0.075	1	1
	1.5	0.006	0.950	1	1
	2	0.093	1	1	1
0.010	1.01	0.011	0.013	0.027	0.167
	1.05	0.016	0.042	0.571	1
	1.1	0.026	0.150	0.993	1
	1.25	0.086	0.891	1	1
	1.5	0.368	0.999	1	1
	2	0.912	1	1	1

p0	w^*/w_{wt}	*w10*	*w30*	*w100*	*w300*
0.0001	1.01	1.00	1.00	1.00	1.00
	1.05	1.00	1.00	1.00	1.05
	1.1	1.00	1.00	1.06	1.1
	1.25	1.00	1.02	1.25	1.25
	1.5	1.00	1.48	1.5	1.5
	2	1.09	2	2	2
0.010	1.01	1.00	1.00	1.00	1.00
	1.05	1.00	1.00	1.03	1.05
	1.1	1.00	1.01	1.10	1.1
	1.25	1.02	1.22	1.25	1.25
	1.5	1.18	1.50	1.5	1.5
	2	1.91	2	2	2

Table S1. Relationship between the relative frequency and relative fitness of a competing clone. The left panel represents deterministic clone frequency dynamics starting from the initial frequency p_0. w^* is the growth rate of the focal clone; w_{wt}, the growth rate of the wild type scaled to 1 and p(t), the frequency of the focal clone after t generations. Gray background denotes the time at which $P > 0.5$. The right panel represents population mean growth rate after t generations. A population composed of 100% wild-type cells has a growth rate of 1; a population composed of 100% focal clones has a growth rate of w^*. Gray background denotes the time at which the mean growth rate reached > 90% of its final value.

References for Supplementary material

1. S. Munevar, Y. Wang, M. Dembo, Traction force microscopy of migrating normal and H-ras transformed 3T3 fibroblasts. *Biophys J* **80**, 1744-1757 (2001).
2. D. B. Lovett, N. Shekhar, J. A. Nickerson, K. J. Roux, T. P. Lele, Modulation of Nuclear Shape by Substrate Rigidity. *Cell Mol Bioeng* **6**, 230-238 (2013).
3. D. C. McFarland, Preparation of pure cell cultures by cloning. *Methods Cell Sci* **22**, 63-66 (2000).
4. M. G. Kenward, J. H. Roger, Small sample inference for fixed effects from restricted maximum likelihood. *Biometrics* **53**, 983-997 (1997).
5. L. E. MacConaill *et al.*, Unique, dual-indexed sequencing adapters with UMIs effectively eliminate index cross-talk and significantly improve sensitivity of massively parallel sequencing. *BMC Genomics* **19**, 30 (2018).
6. H. Li, R. Durbin, Fast and accurate long-read alignment with Burrows-Wheeler transform. *Bioinformatics* **26**, 589-595 (2010).
7. E. Garrison, G. Marth, Haplotype-based variant detection from short-read sequencing. 2012.
8. A. Rodriguez-Palacios *et al.*, Stereomicroscopic 3D-pattern profiling of murine and human intestinal inflammation reveals unique structural phenotypes. *Nat Commun* **6**, 7577 (2015).
9. A. M. Bolger, M. Lohse, B. Usadel, Trimmomatic: a flexible trimmer for Illumina sequence data. *Bioinformatics* **30**, 2114-2120 (2014).
10. D. Kim, B. Langmead, S. L. Salzberg, HISAT: a fast spliced aligner with low memory requirements. *Nat Methods* **12**, 357-360 (2015).
11. Y. Liao, G. K. Smyth, W. Shi, featureCounts: an efficient general purpose program for assigning sequence reads to genomic features. *Bioinformatics* **30**, 923-930 (2014).
12. F. Marini, H. Binder, pcaExplorer: an R/Bioconductor package for interacting with RNA-seq principal components. *BMC Bioinformatics* **20**, 331 (2019).
13. A. Kucukural, O. Yukselen, D. M. Ozata, M. J. Moore, M. Garber, DEBrowser: interactive differential expression analysis and visualization tool for count data. *BMC Genomics* **20**, 6 (2019).
14. S. X. Ge, E. W. Son, R. Yao, iDEP: an integrated web application for differential expression and pathway analysis of RNA-Seq data. *BMC Bioinformatics* **19**, 534 (2018).
15. Y. Liao, J. Wang, E. J. Jaehnig, Z. Shi, B. Zhang, WebGestalt 2019: gene set analysis toolkit with revamped UIs and APIs. *Nucleic Acids Res* **47**, W199-W205 (2019).
16. W. C. Ho, J. Zhang, Evolutionary adaptations to new environments generally reverse plastic phenotypic changes. *Nat Commun* **9**, 350 (2018).